A Potential Role of Acute Choroidal Expansion in Nonarteritic Anterior Ischemic Optic Neuropathy

Andrew J. Feola,[1,2,4] Christopher A. Girkin,[3] C. Ross Ethier,[4] and Brian C. Samuels[3]

[1]Center for Visual and Neurocognitive Rehabilitation, Atlanta VA Medical Center, Atlanta, Georgia, United States
[2]Department of Ophthalmology, Emory Eye Center, Emory University School of Medicine, Atlanta, Georgia, United States
[3]Department of Ophthalmology, University of Alabama at Birmingham, Birmingham, Alabama, United States
[4]Department of Biomedical Engineering, Georgia Institute of Technology/Emory University, Atlanta, GA, United States

Correspondence: Brian C. Samuels, 1670 University Blvd, Volker Hall Room B130, Birmingham, AL 35294, USA;
bsamuels@uabmc.edu.

Received: September 8, 2021
Accepted: February 28, 2022
Published: April 28, 2022

Citation: Feola AJ, Girkin CA, Ethier CR, Samuels BC. A potential role of acute choroidal expansion in nonarteritic anterior ischemic optic neuropathy. *Invest Ophthalmol Vis Sci.* 2022;63(4):23.
https://doi.org/10.1167/iovs.63.4.23

Purpose. Nonarteritic anterior ischemic optic neuropathy (NAION) has been associated with a thickened choroid at the optic nerve head (ONH). Here, we use computational modeling to better understand how choroidal expansion and choroidal geometry influence tissue deformation within the ONH relative to intraocular pressure (IOP) and intracranial pressure (ICP) effects.

Methods. Using a model of the posterior eye that included the sclera, peripapillary sclera, annular ring, pia mater, dura mater, neural tissues, Bruch's membrane, choroid, and lamina cribrosa, we examined how varying material properties of ocular tissues influenced ONH deformations under physiological and supra-physiological, or "pathological," conditions. We considered choroidal expansion (c. 35 µL of expansion), elevated IOP (30 mm Hg), and elevated ICP (20 mm Hg), and calculated peak strains in the ONH relative to a baseline condition representing an individual in the upright position.

Results. Supra-physiological choroidal expansion had the largest impact on strains in the prelaminar neural tissue. In addition, compared to a tapered choroid, a "blunt" choroid insertion at the ONH resulted in higher strains. Elevated IOP and ICP caused the highest strains within the lamina cribrosa and retrolaminar neural tissue, respectively.

Conclusions. Acute choroidal expansion caused large deformations of the ONH and these deformations were impacted by choroid geometry. These results are consistent with the concept that compartment syndrome due to the choroid geometry and/or expansion at the ONH contributes to NAION. Prolonged deformations due to supra-physiological loading may induce a mechanobiological response or ischemia, highlighting the potential impact of choroidal expansion on biomechanical strains in the ONH.

Keywords: choroid, nonarteritic anterior ischemic optic neuropathy, glaucoma, intracranial pressure, ocular biomechanics, computational modeling, finite element modeling

Nonarteritic anterior ischemic optic neuropathy (NAION) is associated with the loss of retinal ganglion cells (RGCs) and sudden vision loss. NAION affects approximately 2.3 to 10.3 people per 100,000 per year with 15% to 24% having subsequent bilateral involvement within 5 years.[1–3] Identifying risk factors for NAION and for bilateral involvement remains a critically unmet need and it is clear that variations in optic nerve head (ONH) morphology are a significant risk factor. Specifically, a characteristic "disc at risk" appearance in the contralateral eye carries a significant risk of NAION. Although the role of the choroid in NAION remains unclear,[1,4] a recent study by Nagia et al. found increased peripapillary choroidal thickness near the ONH in NAION eyes and the unaffected "at-risk" contralateral eyes compared with control subjects.[4]

Given the high rate of bilateral involvement in NAION, there are likely anatomic and/or physiologic similarities between eyes that puts these individuals at risk. As the choroid surrounds the prelaminar tissue compartment through which RGC axons pass, Nagia et al. have hypothesized that NAION may be due to a compartment syndrome.[4,5] The compartment syndrome is thought to potentially develop as choroidal volume fluctuates, which could cause compression in this region resulting in an ischemic cascade.[4] Indeed, human pathology confirms infarction in this region in subjects with NAION,[1,4] and the observed associations of NAION after sleep and sulfide use – both of which can increase choroidal volume – indicate a potential role for choroidal volume changes. However, little is known about how choroidal volume change impacts the prelaminar neural tissue (PLNT). We recently used computational modeling to examine physiological increases in choroidal volume due to the ocular pulse and found that the choroid plays a large and underappreciated role in deformations in the PLNT.[6]

In this study, we use computational modeling to study how variation in choroidal volume impacts ONH deformation relative to physiologic and pathologic variations of intraocular pressure (IOP) and intracranial pressure (ICP). In addition, we considered two geometric models of the

human ONH to better understand how choroidal thickness near the ONH impacts tissue deformations associated with increased choroidal volume and consider its potential impact in NAION pathophysiology.

Methods

Geometry and Finite Element Model

As described previously,[6] we developed two geometric models of the human eye: the first included a "blunt" choroidal termination near the ONH, while the second had a "tapered" termination (Fig. 1). The blunt choroidal geometry had a choroidal thickness of 136 µm over the 500 µm region adjacent to the scleral canal opening, which then thickened to 250 µm.[7–9] The choroid thickness in the tapered geometry increased from 61 µm to 250 µm over the region spanning 125 µm to 2000 µm from the scleral canal opening. The total volume of the choroid in both geometries was 256 µL in the unloaded state.[6,10]

Both geometries incorporated the following tissue regions: posterior sclera, peripapillary sclera, annular scleral ring, lamina cribrosa, PLNT, central retinal vessel, pia mater, dura mater, optic nerve, choroidal tissue, and Bruch's membrane.[6,11,12] The simplified central retinal vessel simulated the effects of a mean arterial pressure (MAP).

Our geometries and meshes were generated in the open-source program Gmsh (V.2.8.3)[13] and our finite element simulations were performed in the finite element solver FEBio.[14] Each geometric model was considered axisymmetric along the center of the central retinal vessel.

Tissue Mechanical Models

Similar to our previous work,[6,12] the posterior sclera, peripapillary sclera, annular ring, pia mater, and dura mater were modeled as neo-Hookean solid matrices with embedded collagen fibers following von Mises distributions.[15,16] In the posterior sclera, pia mater and dura mater the fibers were distributed as planar isotropic ($k_f = 0$).[17,18] In the peripapillary sclera and annular ring, the fibers were oriented circumferentially ($k_f = 0.85$ and 1.85, respectively).[18] For the above tissues, we defined four additional coefficients to describe each tissue's mechanical behavior (Supplementary Table S1). One coefficient described the stiffness of the ground substance (c_1), representing all tissue constituents except the collagen fibers (e.g. proteoglycans, cells, elastin, etc.). The coefficients c_3 and c_4 defined the stiffness of the collagen fibers, and we set the bulk modulus to enforce tissue incompressibility (K = 100 MPa).

The lamina cribrosa, optic nerve, central retinal vessel, PLNT, and Bruch's membrane were modeled as linear-elastic, isotropic, and homogeneous, requiring two coefficients to describe each tissue's mechanical behavior: Young's modulus (E) and Poisson ratio (ν). Young's modulus values were adopted from previous experimental and

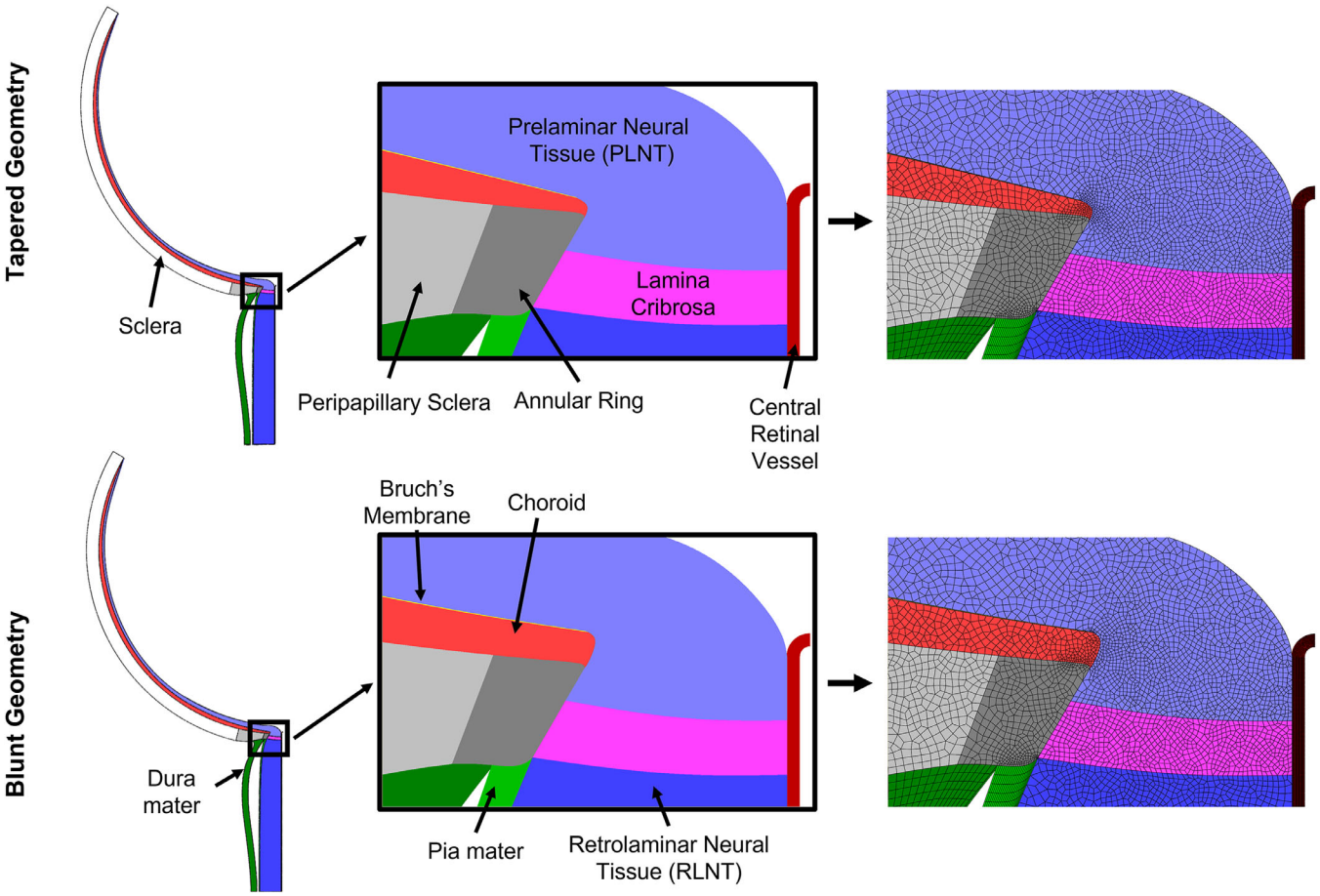

Figure 1. Two geometric models used for finite element simulations of ONH biomechanics, with each tissue component identified. The top and bottom rows display the tapered and blunt choroid anatomies, respectively. The left image shows the overall geometry, the middle shows a zoomed image of the ONH, and the right shows the finite element mesh at the ONH.

Investigative Ophthalmology & Visual Science

Table. Overview of the Loading Conditions for Finite Element Simulations

Abbreviation	IOP (mm Hg)	ICP (mm Hg)	Choroid Volume Change (µL)
Physiological loading conditions			
ΔV = 2.2 µL	15	0	2.2
ΔV = 6.4 µL	15	0	6.4
ΔV = 14 µL	15	0	14
Physiological IOP	19	0	0
Physiological ICP	15	10	0
Supra-physiological loading conditions			
ΔV = 32 µL	15	0	32
ΔV = 35 µL	15	0	35
Elevated IOP	30	0	0
Elevated ICP	15	20	0

All peak strains reported for the physiological and supra-physiological loading conditions are relative to the Baseline (reference) loading conditions of an individual in an upright position (IOP = 15 mm Hg, ICP = 0 mm Hg, and ΔV = 0 uL).

computational studies of the posterior eye.[19,20] We assumed that the neural tissue (e.g. the prelaminar neural tissue and optic nerve) were partially compressible ($\nu = 0.45$), while the remaining tissues were nearly incompressible ($\nu = 0.49$).[12,19]

As we detailed previously,[6] the choroid was represented as a mixture material comprised of a linear-elastic solid matrix capable of swelling based on the Donnan equilibrium, which allows a prescribed volume change (i.e. expansion) through a single coefficient (c_o^F). This coefficient is only a phenomenological means to govern tissue volume and does not directly represent blood flow or perfusion within the choroid. We report the Donnan equilibrium swelling as choroidal expansion (see Supplementary Table S1).

Physiological Loading Conditions

To simulate a baseline (reference) configuration we specified 3 pressures: IOP = 15 mm Hg; ICP = 0 mm Hg, corresponding to an upright position; and MAP = 57 mm Hg. We also specified no choroidal expansion (i.e. a change in choroidal volume ΔV = 0 µL). To investigate the impact of physiological choroidal expansion, we specified the same pressure loads as our baseline condition while varying choroidal volume over a cardiac cycle. As previously described,[6] we estimated that the change in choroidal volume associated with the ocular pulse is 2.2 µL to 14.2 µL (ΔV = 2.2, 6.4 and 14 µL).[21–23] We also examined a physiological variation of IOP from 15 to 19 mm Hg as might be expected to occur due to normal diurnal variation (ΔIOP = 4 mm Hg).[12] Additionally, we simulated an increase in ICP to 10 mm Hg (ΔICP = 10 mm Hg), corresponding to a change from the upright to the supine position.[24–26] In the above physiological loading conditions of IOP and ICP, we did not specify any choroidal expansion (ΔV = 0 µL). For simplicity, we refer to the 5 physiological loading conditions by the primary parameter being investigated: 1) ΔV = 2.2 µL, 2) ΔV = 6.4 µL, 3) ΔV = 14 µL, 4) IOP = 19 mm Hg, and 5) ICP = 10 mm Hg (Table). Each physiological loading condition was applied separately to the baseline (reference) configuration.

Supra-Physiologic or Pathologic Loading Conditions

We then examined supra-physiologic, or "pathological," levels of choroidal expansion relative to elevated IOP and elevated ICP. For supra-physiological levels of choroidal expansion, we estimated choroidal volume of 32 and 35 uL based on the choroidal thickness observed in subjects with NAION.[4,27] In brief, we used choroidal thicknesses that were reported at locations from 100 µm to 3000 µm starting at the scleral canal opening of eyes affected by NAION.[4,27] We then estimated the degree of choroidal expansion as the difference in choroidal volume between healthy subjects and subjects with NAION. For elevated IOP that simulated a glaucomatous condition, we increased IOP to 30 mm Hg without any choroidal expansion.[28] Finally, we compared the impact of elevated ICP (ICP = 20 mm Hg) to simulate pathological levels of ICP associated with idiopathic intracranial hypertension (IIH).[29–33] An overview of the four separate supra-physiological loading conditions is displayed in the Table and are referred to by the parameter being investigated: 1) ΔV = 32 µL, 2) ΔV = 35 µL, 3) IOP = 30 mm Hg, and 4) ICP = 20 mm Hg. Similar to the physiological conditions, each supra-physiological loading condition (i.e. IOP, ICP, or ΔV) was applied individually. We did not consider situations in which two changed loads were simultaneously applied.

Finite Element Modeling Estimated Strain Range due to Biomechanical Variability

Tissue material properties impact the biomechanical behavior of any tissue and will impact ONH deformations.[6,11,12,19] To investigate the effects of impact of variation in tissue properties across each of the above loading conditions (5 physiological and 4 supra-physiological), we varied tissue material properties using a Latin Hypercube Sampling (LHS) approach.[34,35] The range of LHS allows us to define the specific distribution and range of each input parameter to the simulations. The range of LHS allows us to define the specific distribution and range of each input parameter to the simulations. The range for each input parameter was based on values reported by Sigal et al.[11,12] All 21 tissue material properties were assumed to follow uniform distributions. Adopting this approach from our earlier work,[12] we determined that 200 simulations per loading condition per geometry were required to suitably represent a simulated population.

Outcome Measures

Our outcome measures were the computed strains in three ONH tissues[6,12]: the PLNT (defined as tissue within 1 mm of the anterior lamina cribrosa surface), lamina cribrosa, and retrolaminar neural tissue (RLNT; defined as optic nerve tissue within 1 mm of the posterior lamina cribrosa surface). Strain is a measure of normalized tissue deformation, and it can be represented as a second order tensor with three principal components, namely a first, second, and third principal strain. We computed the peak first and third principal strains, which were defined as the 95th and 5th percentile strain, respectively. The peak first principal strain refers to the peak tension, or stretch, the tissue experiences, whereas

Investigative Ophthalmology & Visual Science

the peak third principal strain relates to the peak compression experienced by the tissue.

We used the "relative displacement" method to account for the effects of prestress in ocular tissues relative to our baseline condition, or reference condition.[35,36] In brief, the first step brought the model to our baseline condition (IOP = 15 mm Hg, ICP = 0 mm Hg, MAP = 57 mm Hg, and ΔV = 0 µL). The resulting state of the model was taken as the reference for all subsequent strain calculations. This allowed us to understand how physiological and supra-physiological conditions affected peak strains in the ONH.

Statistics

The peak first and third principal strains in the PLNT, lamina cribrosa, and RLNT were collected for each simulation (n = 200 each) and loading conditions (5 physiologic and 4 supra-physiologic), resulting in a total of 1,800 values of peak tensile and compressive strains for each tissue region. To compare the distributions of the peak strains between loading conditions *within* each geometry we used a Kruskal-Wallis test and performed a pairwise comparison between each condition. To account for multiple Kruskal-Wallis tests, we applied a Bonferroni correction ($\alpha = 0.05/12 = 0.004$) to account for each tissue region, peak strain, and choroid geometry. Within each Kruskal-Wallis test, we performed a Dunn's correction and set a significance threshold of $P = 0.01$. To compare *between* each geometry, we performed a 2-way ANOVA to examine the impact of geometry and loading condition on peak strains. To account for multiple tests for each peak strain in each region (6 tests) we performed a Bonferroni correction to the initial significance threshold ($\alpha = 0.05/6 = 0.008$). To account for multiple comparisons within each ANOVA we used a Sidak post hoc with a $P = 0.01$.

Results

Physiological and Supra-Physiological Loading

We observed a different profile of deformation at the ONH for each loading condition, and this profile became more exaggerated under supra-physiological loads (Figs. 2 and 3). We found a range of peak tensile and compressive strains as tissue material properties were varied under physiological loading conditions. Because peak tensile and compressive strains showed comparable trends, we discuss those trends collectively as "peak strains" unless otherwise stated. The PLNT, lamina cribrosa, and RLNT were differentially affected by physiologic levels of choroidal expansion, IOP and ICP (significance levels shown in Supplementary Tables S2–S7). Under physiological conditions, choroidal expansion increased peak strains within the PLNT in both the blunt and tapered ONH geometries, and these strains were greater than the strains associated with physiological changes in IOP and ICP (Figs. 4 and 5). For example, the peak strains in the PLNT were significantly larger after choroidal volume changes of 6.4 µL and 14 µL for both geometries than were the strains due to physiological variation in IOP and ICP (see Supplementary Tables S2, S3). In the lamina cribrosa, IOP and ICP increases impacted the peak strains more than choroidal expansion when the volume change was less than or equal to 6.4 µL, but choroidal volume changes of 14 µL led to peak strains that were not significantly different compared to strains due to normal variations in IOP and ICP (see Supplementary Tables S4, S5). Within the RLNT, the ICP was noted to be the primary driver of peak strain. Physiological changes in ICP resulted in peak strains that were significantly greater than those caused by IOP and choroidal volume changes (see Supplementary Tables S6, S7).

Under supra-physiological, or pathological, conditions there was a wider range of strains relative to those expected

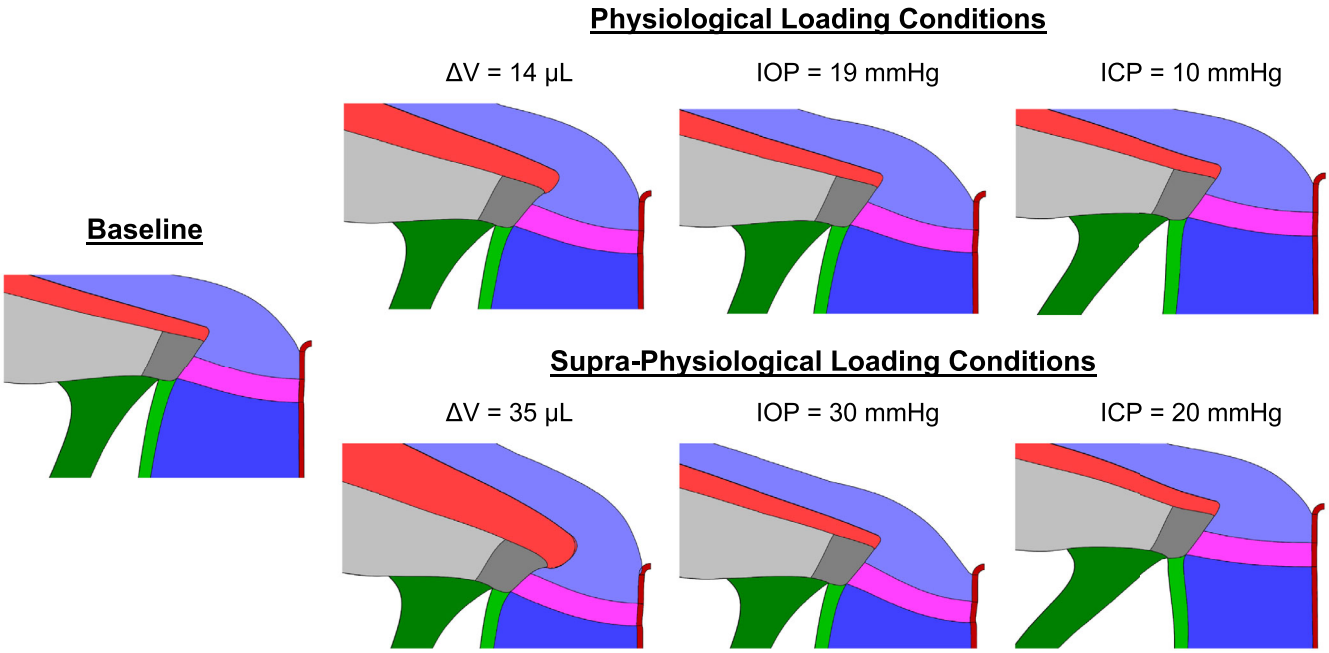

Figure 2. Tissue deformations for the blunt choroid geometry under physiological (top) and supra-physiological (lower) loading conditions relative to the baseline (prestressed) condition in the left-hand column. The swollen choroid intrudes into the ONH, whereas the PLNT is compressed by elevated IOP and the optic nerve sheath expands due to elevated ICP. All deformations are magnified 10 times for easier visualization.

Investigative Ophthalmology & Visual Science

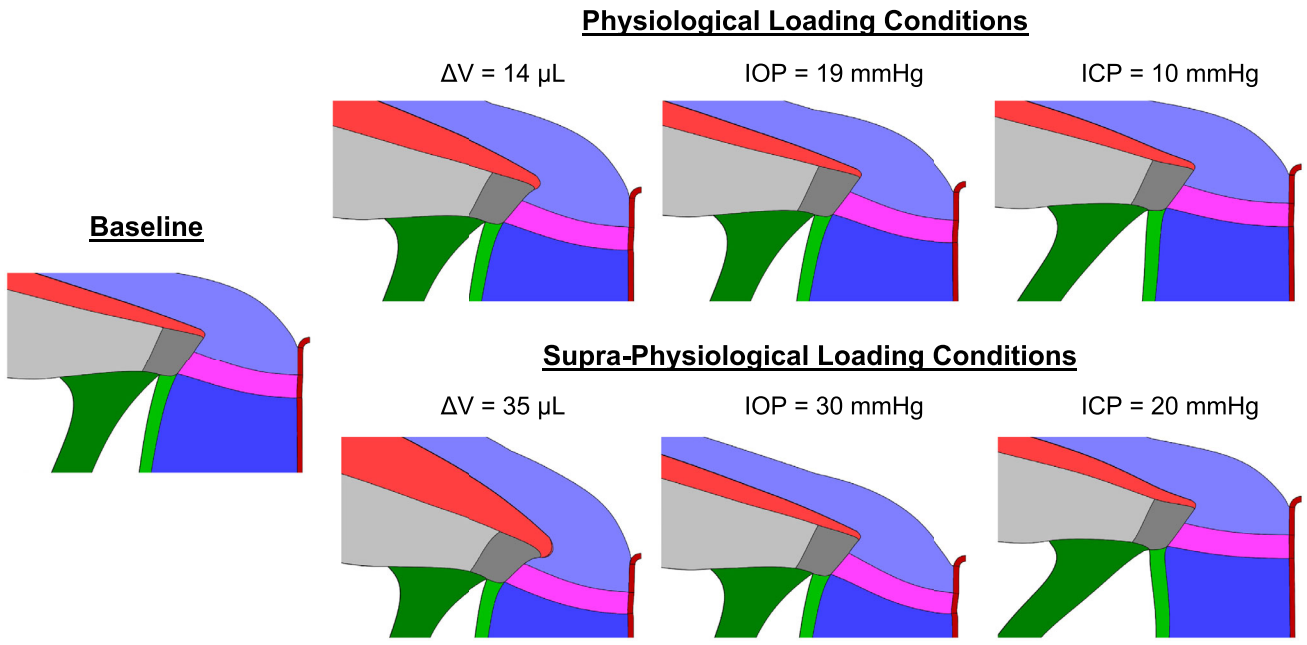

Figure 3. Tissue deformations for the tapered choroid geometry under physiological (top) and supra-physiological (lower) loading conditions relative to the baseline (prestressed) condition. For interpretation of plots, see Figure 2. All deformations are magnified 10 times for easier visualization.

to occur due to physiological choroidal expansion, IOP, and ICP (Figs. 6 and 7; note the differences in the y-axis compared to Figs. 4 and 5). In the PLNT, we found that changing choroidal volume to that found in subjects with NAION significantly increased the peak tensile strains, as well as the range of peak strains, compared to elevated IOP and ICP. In the PLNT, a few simulations of elevated IOP caused peak compressive strains within a similar range of those seen with pathologic choroidal volume changes. However, the distribution of peak compressive strains caused by elevated IOP was significantly lower than those due to supra-physiological choroidal expansion. Within the lamina cribrosa, elevated IOP caused the highest peak strains compared to all levels of choroidal expansion and ICP. Finally, elevated ICP caused significantly higher peak tensile strains in the RLNT compared to pathologic volume changes in the choroid and to changes in the IOP; however, peak compressive strains induced by elevated IOP and ICP were not significantly different ($P = 1.0$). In the PLNT, excluding the comparisons between elevated IOP and ICP to choroidal expansion less than or equal to 6.4 μL, all pathological conditions within a geometry (i.e. blunt or tapered) led to significantly higher peak strains compared to the physiological loading conditions (see Supplementary Tables S2, S3).

Blunt Versus Tapered Choroidal Geometry

In the PLNT, we found that choroidal expansion resulted in significantly larger peak strains in the blunt geometry compared to the tapered geometry (see Supplementary Fig. S1; $P < 0.0001$). In the lamina cribrosa, choroidal expansion within the physiological range was not significantly different between the geometries (see Supplementary Fig. S2); however, peak strains were significantly higher in the lamina cribrosa in the blunt geometry for levels of choroidal volumes associated with NAION ($P < 0.0001$ for each comparison). In the RLNT, we observed no significant differences in the peak tensile strains between the blunt and tapered geometry due to choroidal expansion. We did observe higher peak compressive strains in the RLNT due to choroidal volume changes of 32 μL ($P = 0.0004$) and 35 μL ($P = 0.0002$) in the blunt geometry compared to the tapered geometry (see Supplementary Fig. S3). We found no significant differences in the peak strains between the two ONH geometries in any of the tissue regions (PLNT, lamina cribrosa, or RLNT) due to physiological or supra-physiological levels of IOP and ICP loading conditions. Finally, we found a small change in choroidal volume due to changes in IOP and ICP (see Supplementary Fig. S4). These choroidal volume changes were similar across choroidal geometries and were less than 0.5% of the total choroidal volume.

Discussion

Choroidal geometry and volume have been proposed to play a role in NAION.[4,5,9] Compared to elevated IOP, the role of choroidal geometry and supra-physiological levels of choroidal expansion on ONH biomechanics has received less attention.[6,37,38] Here, we observed that supra-physiological choroidal expansion to volumes seen in subjects with NAION caused significantly larger peak strains in the PLNT compared to strains caused by elevation of IOP or ICP. These results suggest that choroidal volume changes associated with NAION are a potential source of significant deformation on ONH tissues (see Figs. 4–7).[39–41]

In our previous study, we examined ONH deformation due to physiological choroidal volume changes. We then performed a sensitivity analysis to characterize how variation in physiological changes in ONH pressures (IOP, ICP, and MAP) within the physiologic range of a simulated subject in the upright position, tissue material properties,

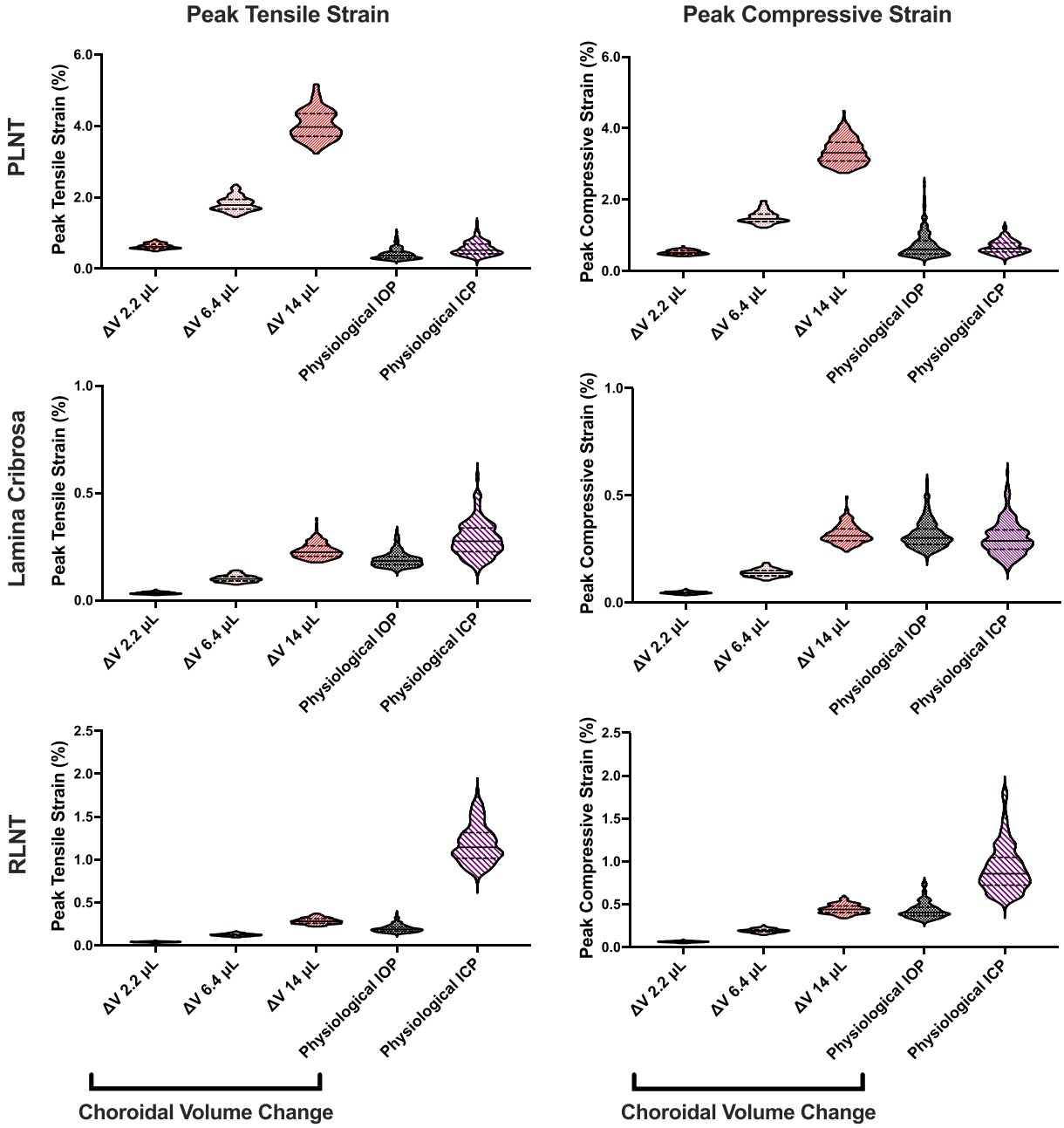

Figure 4. Violin plots of the peak tensile (left column) and peak compressive (right column) strains estimated to occur under physiological loading conditions in the blunt choroid geometry. The distribution of peak strains is a result of varying tissue material properties (Supplementary Table S1) at each loading condition, as quantified through Latin Hypercube simulation. The peak strains varied widely depending on the loading condition and ONH region; notably, the range of predicted peak strains in the PLNT was strongly influenced by choroidal expansion. Significance values are provided in Supplementary Tables S2, S4, and S6. In these violin plots, the center line represents the mean and the dashed lines represent the interquartile range.

blunt insertion of the choroid.[6] We found that choroidal swelling and geometry influenced deformation in the PLNT and that each ONH region (PLNT, lamina cribrosa, and RLNT) had specific factors that most impacted deformation. These were important findings; however, there were several aspects we did not consider in that work. For example, we did not examine supra-physiological levels of choroidal swelling, elevated IOP, or elevated ICP, which may be important for glaucoma, idiopathic intracranial hypertension, and NAION. In addition, we did not consider how IOP, ICP, and choroidal swelling differentially influence deformation in each region of the ONH; nor did we account for the potentially important effect of prestress in ocular tissues.[36] Thus, our present approach: 1) accounted for prestress in tissues; 2) assessed the effects of physiological changes in IOP, ICP, and choroidal swelling; and 3) examined supra-physiological loading levels of IOP, ICP, and choroidal swelling. This enabled us to better compare choroidal volume changes associated with NAION to elevated IOP and elevated ICP.

Currently, the exact cause of NAION remains unclear. For some time, it was thought that a small optic disc size

Investigative Ophthalmology & Visual Science

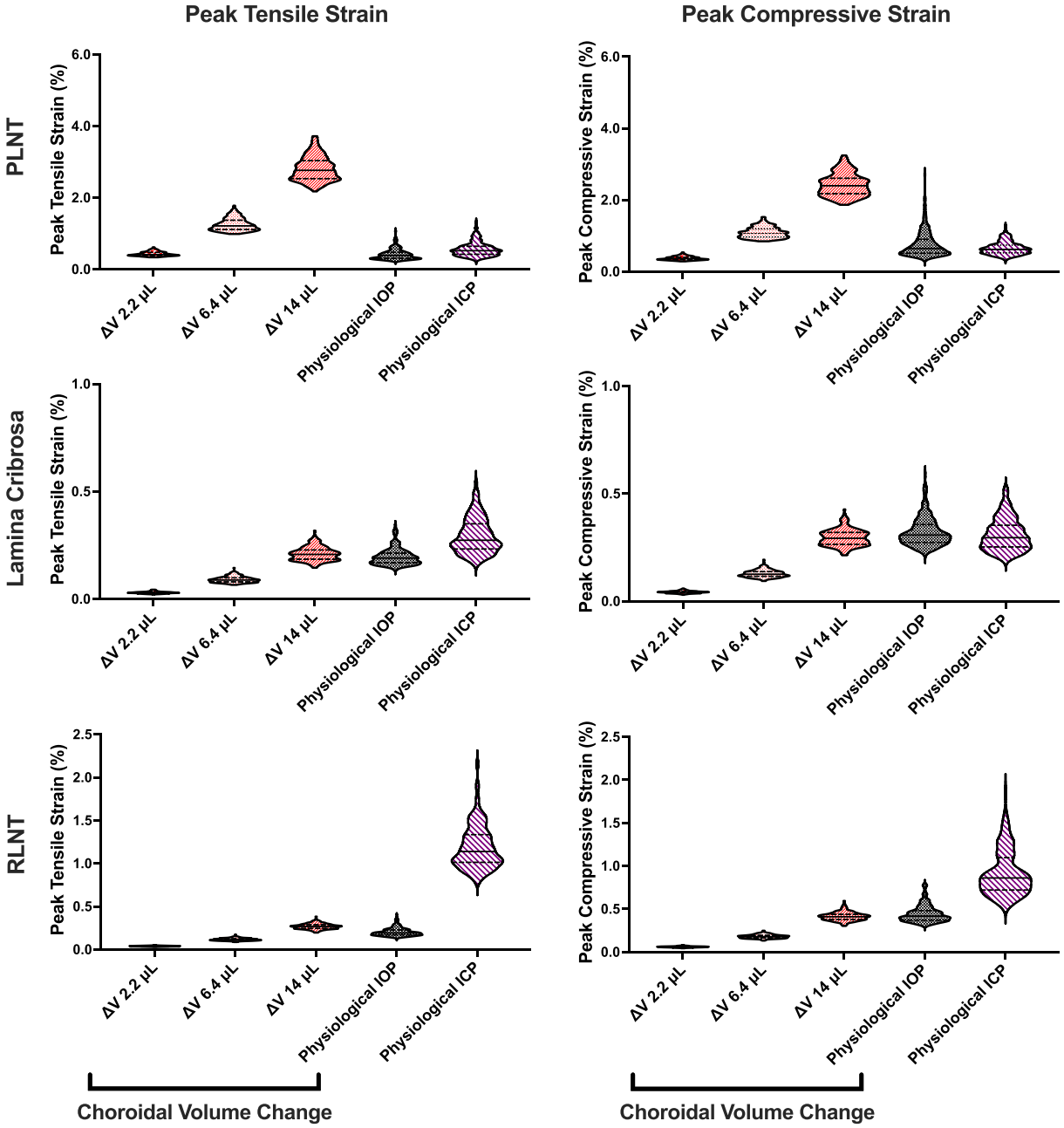

Figure 5. Violin plots of the peak tensile (left column) and peak compressive (right column) strains estimated to occur under the physiological loading conditions in the tapered choroid geometry. For interpretation of plots, see Figure 4.

observed on clinical ophthalmoscopy led to axons of the retinal ganglion cells being crowded within the disc,[42] resulting in the classic "disc-at-risk" appearance. It was thought that the small disc and subsequently crowded axons were particularly susceptible to some unknown NAION-inducing insult. However, subsequent optical coherence tomography (OCT) studies have shown that the size of Bruch's membrane opening in subjects with NAION were similar to disc size in age-matched controls.[43–45] An alternative hypothesis that has been proposed by Girkin and colleagues is that a PLNT compartment syndrome is induced by expansion of the thicker circumpapillary choroid leading to capillary nonperfusion, prelaminar tissue ischemia, tissue edema, and eventual infarction of the axons in the PLNT region.[4,5] This theory is supported by Tesser and colleagues' histologic findings of PLNT ischemia in patients with NAION.[41] Our data (see Figs. 6 and 7) further support this theory. We found that a change in choroidal expansion to 32 µL to 35 µL results in peak tensile and compressive strains between 7.5% and 12% in the PLNT, and computational simulations may underestimate the level of tissue deformation.[46] For comparison, these strains are an order of magnitude greater than strains seen in the PLNT and lamina cribrosa caused by an elevation of IOP to 30 mm Hg. Additionally, the anatomy itself was found to play an important role, where significantly larger PLNT strains occurred in the blunt compared to the tapered choroid geometry under both physiological and supra-physiological levels of choroidal expansion (see

Investigative Ophthalmology & Visual Science

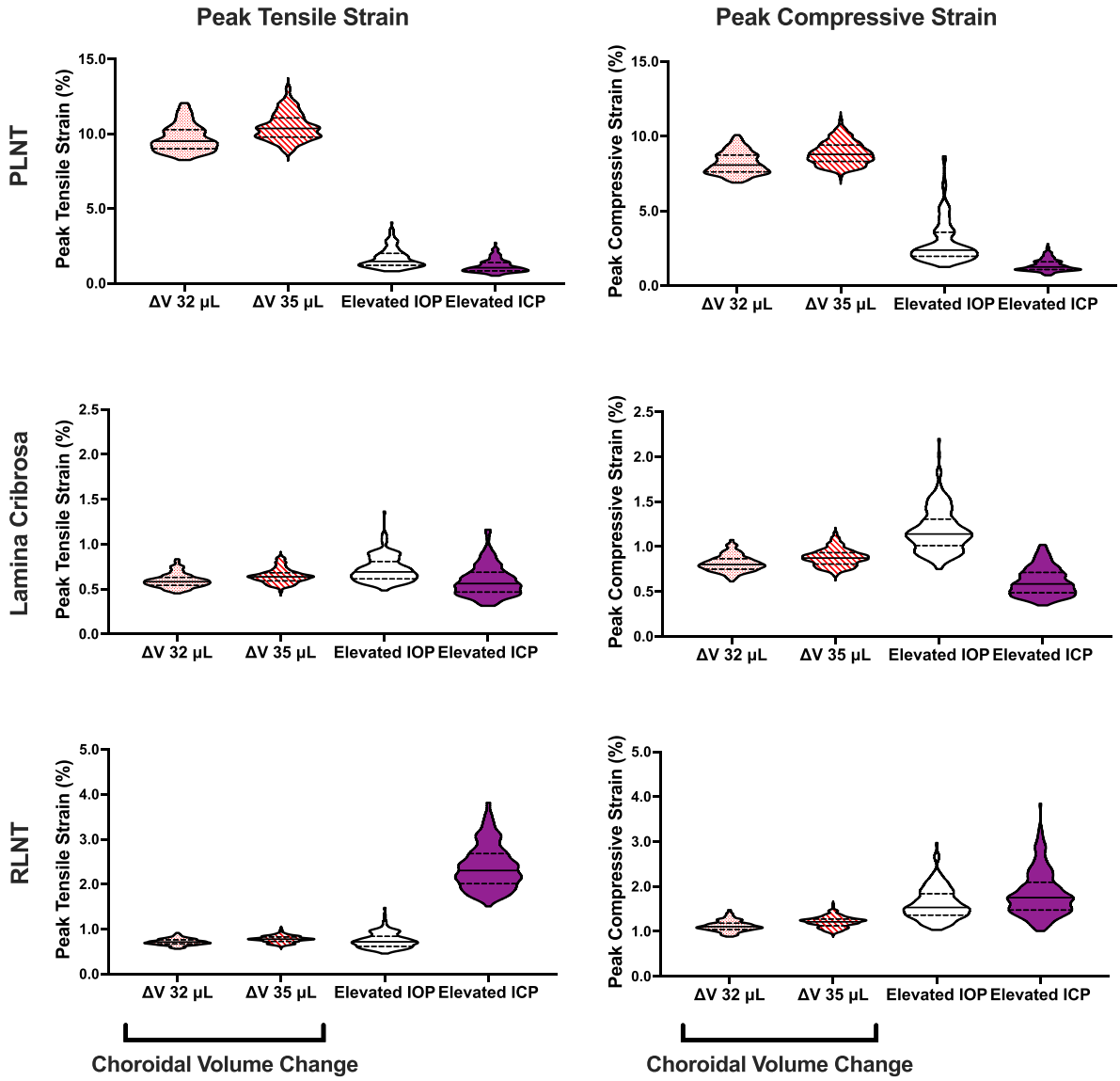

Figure 6. Violin plots of the peak tensile (left column) and peak compressive (right column) strains estimated to occur at each loading condition in the blunt choroid geometry. For interpretation of plots, see Figure 4. Note the different axis scales as compared to Figures 4 and 5.

Supplementary Fig. S1). Thus, the data obtained by Girkin and colleagues[4] showing that the peripapillary choroid adjacent to the optic nerve head (0–250 µm) is significantly thicker than normal controls (similar to our blunt geometry) become more significant. Extrapolating our findings to this data, one can infer that the anatomy of subjects with NAION predisposes them to larger PLNT strains for a given choroid volume change compared to normal subjects. This could put them at higher risk for NAION if a PLNT compartment syndrome plays a role in the pathogenesis of NAION.

Our results also demonstrate that the impact of IOP and ICP under physiological and supra-physiological ranges was not different between the different choroid geometries; however, the blunt choroidal geometry near the ONH resulted in higher peak strains in the PLNT at each level of choroidal expansion compared to the tapered choroid insertion. These results support the concept that choroidal geometry, or potential crowding near the ONH, plays a vital role in NAION pathophysiology. Although these studies cannot determine if this strain is sufficient to induce capillary nonperfusion and initiate the feedback loop resulting in ischemic optic neuropathy, it serves as strong proof-of-concept.

ONH as a Dynamic Loading Environment

These simulations are also the first, to our knowledge, that estimate tissue strains in the ONH caused by changes in choroidal volume, IOP, and ICP over a broad range of both physiologic and pathologic levels. The ONH is situated in a complex and dynamic biomechanical environment.[6,37,47,48] Further, the altered mechanical loading and tissue properties experienced by the ONH are proposed to be involved in the pathogenesis and/or progression of multiple eye conditions, including glaucoma, IIH, NAION, and Spaceflight Associated Neuro-ocular Syndrome (SANS).[4,9,47–49] Importantly,

Investigative Ophthalmology & Visual Science

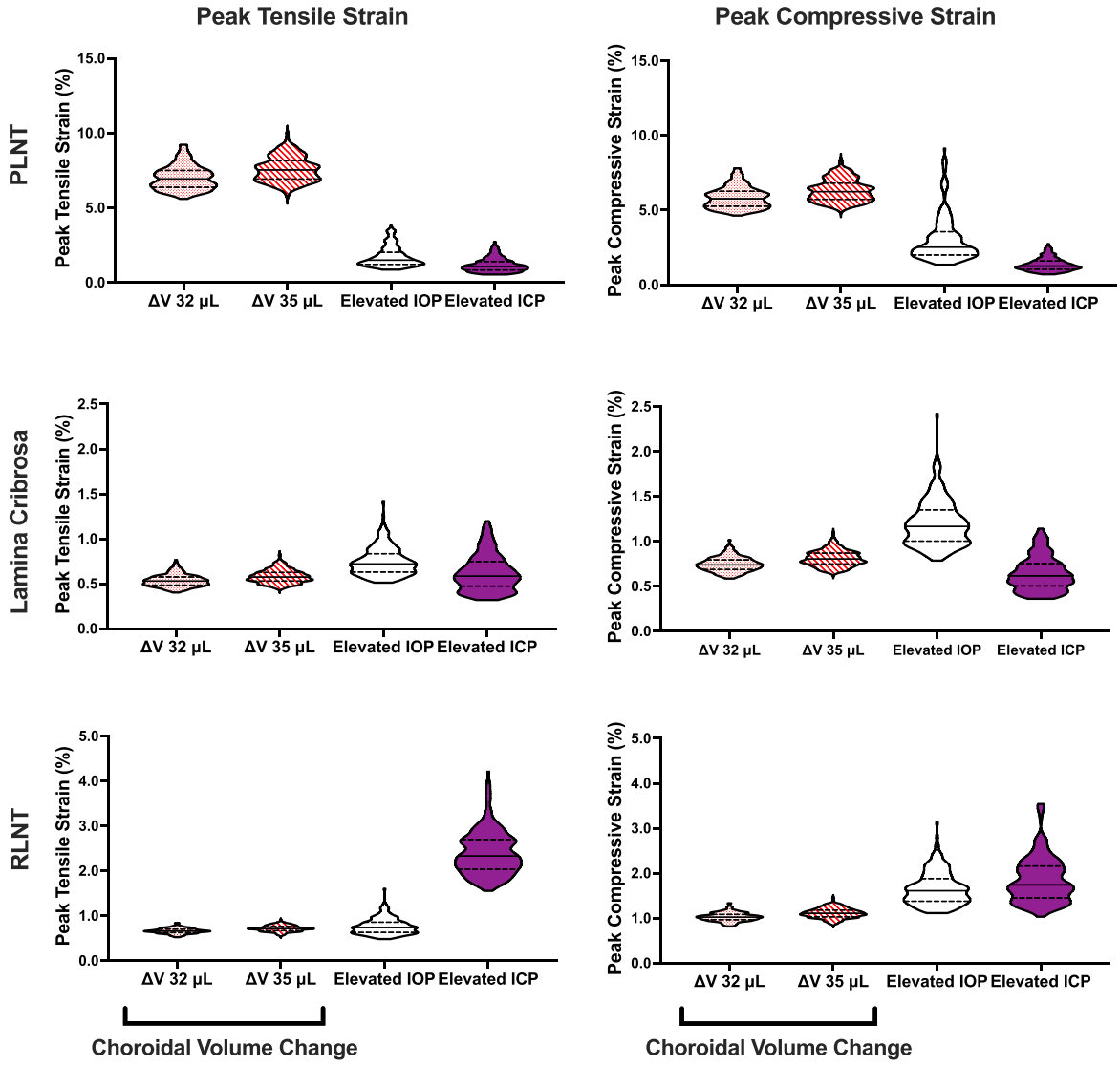

Figure 7. Violin plots of the peak tensile (left column) and peak compressive (right column) strains estimated to occur at each loading condition in the tapered choroid geometry. For interpretation of plots, see Figure 4. Note the different axis scales as compared to Figures 4 and 5.

glaucoma, IIH, and NAION are all associated with changes in IOP, ICP, and choroidal volume, respectively.[28–33]

These results provide valuable insight when considering mechanisms that could play a role in the development or progression of these various ophthalmic pathologies. Our studies provide evidence that physiologic changes in choroidal volume add to the dynamic nature of the ONH environment. The PLNT was largely impacted by choroidal volume changes and IOP. The lamina cribrosa is directly influenced by IOP and, as expected, fluctuations in ICP were the primary driver of the dynamic forces in the RLNT.

It is likely that pathologic choroidal expansion or chronic abnormal thickening of the choroid predisposes individuals to NAION that leads to loss of RGCs, retinal damage, and sudden loss of vision. Our data show convincing evidence that supra-physiological levels of choroidal expansion cause high peak strains in the PLNT and lamina cribrosa. However, similar to the transient changes in IOP, physiologic choroidal volume is not static and varies with ocular pulse pressure, blinks, or saccades[50,51] in addition to changes in fluid distribution with body position or with sildenafil use. These later factors result in a more sustained choroidal expansion and are also risk factors for NAION. These data further suggest that transiently elevation of PLNT deformation may develop in the eye predisposed to NAION with a pathologically thickened choroid.

Limitations

Our work has several limitations. It has been proposed that NAION is related to choroidal geometry at the ONH; thus, examining multiple choroidal geometries would be advantageous. Here, we only included two geometries in which the choroid varied only near the ONH. This is an oversimplification of the choroid's complex geometry and the variations in choroid geometry. A second limitation was the use of an axisymmetric geometric model to represent the complex anatomy of the eye. Such axisymmetric models

Investigative Ophthalmology & Visual Science

cannot capture the complex variations in choroidal, retinal, and scleral thicknesses between different regions.[4,7,8] Here, we used average choroidal thicknesses to represent a generic eye geometry. The present study motivates future work aimed at developing subject-specific geometries of the choroid near the ONH in control subjects and patients with NAION to estimate differences in deformations within ONH tissues and potentially identify "at risk" geometries or other biomarkers for NAION. Ideally, these will be full 3D geometries based on subject-specific information obtained from OCT or serial histological sectioning. However, even with the above-mentioned simplifications, this work highlights the importance of choroidal expansion under physiological and supra-physiological loading and ONH geometries.

Another concern of our study is the limited understanding of temporal component of choroidal volume changes in patients with NAION. Here, we used choroidal thickness measurements from patients with NAION to estimate a choroidal volume change in our geometric models.[4,9] The current approach models the impact of an acute change in choroidal volume on ONH deformation, but it is unknown whether patients with NAION have acute volume choroidal changes or whether they have chronically thickened choroids and other concomitant factors increase their risk for NAION. Understanding this temporal component will be critical to identifying biomarkers for NAION risk. Although the temporal component may not be understood for NAION, our findings remain highly relevant to other pathologies (e.g. SANS) known to have acute choroidal volume changes. Thus, it is likely that the choroid still plays a role in the mechanical environment of the ONH.

Another limitation is that our approach does not model the interplay between IOP and choroidal volume. Instead, we independently alter choroidal volume and IOP in physiological and supra-physiological loadings for purposes of our parametric study. An alternative approach exists that examines the interplay of these effects,[37] but our approach is appropriate for identifying the importance of each loading (e.g. IOP, ICP, and ΔV) on ONH deformation. In this study, we also examined the independent effect of choroidal swelling on PLNT deformation; however, it is possible that choroidal swelling in NAION is related to altered blood perfusion which could also impact swelling in the PLNT. There may also be a dynamic aspect in NAION, with varied blood perfusion and PLNT thickness throughout the time course of the disease.[52–55] Unfortunately, we do not fully understand the relationship and interplay between PLNT thickening, blood perfusion, and choroidal volume, which makes it extremely challenging to accurately incorporate such effects into our model. Future models should consider how these parameters interact with each other.

Finally, similar to other finite element modeling studies, we made assumptions about the properties of the connective tissues within the posterior eye. In brief, we assumed that several of the softer tissues were linear, elastic, isotropic, and incompressible, which does not truly represent their complex behavior. To ensure that using a linear elastic material for these specific tissues did not significantly affect results, we re-ran a simulation using our blunt choroid geometry and a swelling of 35 µL using a hyper-elastic Neo-Hookean material instead of the linear-elastic constitutive model. The largest difference we found was 0.87% in the peak compressive of the PLNT, which was a relatively small effect. Therefore, we do not believe our choice of material for these tissues significantly impacted our results or interpretation. In addition, it is known that these constitutive relationships do not truly represent the complex behavior of these tissues. For example, the lamina cribrosa consists of collagen fibers that have a high degree of anisotropic behavior, and limited information exists regarding the material properties of Bruch's membrane, which is the main barrier between the PLNT and choroid.[20,56] The thinness of, and limited access to, Bruch's membrane makes it difficult to experimentally characterize, although it likely plays an important role in influencing the impact of choroidal expansion on ONH deformation. Finally, it is also challenging to determine the material properties of the choroid and our models are likely a simplification of its mechanical behavior. Fortunately, our model aimed to examine the impact of choroidal expansion on the surrounding tissues (PLNT, lamina cribrosa, and RLNT) and not the choroid itself. Therefore, we were able to choose a simpler material model for the choroid in which we could impose choroidal volume changes (e.g. expansion).

Summary

Despite the limitations noted above, we were able to examine how acute choroid expansion to volumes seen in subjects with NAION and choroidal geometry influence strains in the ONH under physiological and supra-physiological conditions. These results agree with our previous work,[6] strongly suggesting that the choroid plays an important role in ONH deformation even relative to elevated IOP and ICP. Further, we identified that choroid geometry plays a role in deformation of the PLNT and potentially is a factor for developing a compartment syndrome within the ONH. Understanding how choroidal geometry and expansion may be related remains an important goal in understanding NAION, and our findings motivate future studies to better understand the role of choroidal expansion in ONH biomechanics and tissue function, particularly in pathologies where choroidal engorgement has been identified, including NAION, IIH, and SANS.

Acknowledgments

Supported by a Department of Veterans Affairs Rehabilitation Research & Development (RR&D) Service Career Development Award (RX002342A; to A.J.F.), the Georgia Research Alliance (C.R.E.), and an unrestricted Research to Prevent Blindness grant (B.C.S. and C.A.G.), EyeSight Foundation of Alabama (C.A.G.).

Disclosure: **A.J. Feola**, None; **C.A. Girkin**, None; **C.R. Ethier**, None; **B.C. Samuels**, None

References

1. Hattenhauer MG, Leavitt JA, Hodge DO, Grill R, Gray DT. Incidence of nonarteritic anterior ischemic optic neuropathy. *Am J Ophthalmol*. 1997;123:103–107.
2. Johnson LN, Arnold AC. Incidence of nonarteritic and arteritic anterior ischemic optic neuropathy. Population-based study in the state of Missouri and Los Angeles County, California. *J Neuroophthalmol*. 1994;14:38–44.
3. Newman NJ, Scherer R, Langenberg P, et al. The fellow eye in NAION: report from the ischemic optic neuropathy decompression trial follow-up study. *Am J Ophthalmol*. 2002;134:317–328.

4. Nagia L, Huisingh C, Johnstone J, et al. Peripapillary Pachychoroid in Nonarteritic Anterior Ischemic Optic Neuropathy. *Invest Ophthalmol Vis Sci*. 2016;57:4679–4685.
5. Girkin CA. Is Nonarteritic Ischemic Optic Neuropathy Due to Choroidal Compression of the Prelaminar Neurovascular Compartment of the Optic Nerve Head? *J NeuroOphthalmol*. 2018;38:1–3.
6. Feola AJ, Nelson ES, Myers J, Ethier CR, Samuels BC. The Impact of Choroidal Swelling on Optic Nerve Head Deformation. *Invest Ophthalmol Vis Sci*. 2018;59:4172–4181.
7. Hirata M, Tsujikawa A, Matsumoto A, et al. Macular choroidal thickness and volume in normal subjects measured by swept-source optical coherence tomography. *Invest Ophthalmol Vis Sci*. 2011;52:4971–4978.
8. Lee KM, Lee EJ, Kim TW. Juxtapapillary choroid is thinner in normal-tension glaucoma than in healthy eyes. *Acta Ophthalmologica*. 2016;94:e697–e708.
9. Rhodes LA, Huisingh C, Johnstone J, et al. Peripapillary choroidal thickness variation with age and race in normal eyes. *Invest Ophthalmol Vis Sci*. 2015;56:1872–1879.
10. Kiel JW. Choroidal myogenic autoregulation and intraocular pressure. *Exp Eye Res*. 1994;58:529–543.
11. Sigal IA, Flanagan JG, Ethier CR. Factors influencing optic nerve head biomechanics. *Invest Ophthalmol Vis Sci*. 2005;46:4189–4199.
12. Feola AJ, et al. Finite Element Modeling of Factors Influencing Optic Nerve Head Deformation Due to Intracranial Pressure. *Invest Ophthalmol Vis Sci*. 2016;57:1901–1911.
13. Geuzaine CR, Remacle J-F. Gmsh: a three-dimensional finite element mesh generator with built-in pre- and post-processing facilities. *Intl J Numerical Methods Engineering*. 2009;79:1309–1331.
14. Maas SA, Ellis BJ, Ateshian GA, Weiss JA. FEBio: finite elements for biomechanics. *J Biomechanical Engineering*. 2012;134:011005.
15. Girard MJ, Suh JK, Bottlang M, Burgoyne CF, Downs JC. Biomechanical changes in the sclera of monkey eyes exposed to chronic IOP elevations. *Invest Ophthalmol Vis Sci*. 2011;52:5656–5669.
16. Gouget CL, Girard MJ, Ethier CR. A constrained von Mises distribution to describe fiber organization in thin soft tissues. *Biomechanics and Modeling in Mechanobiology*. 2012;11:475–482.
17. Girard MJA, Dahlmann-Noor A, Rayapureddi S, et al. Quantitative mapping of scleral fiber orientation in normal rat eyes. *Invest Ophthalmol Vis Sci*. 2011;52:9684–9693.
18. Coudrillier B, Boote C, Quigley HA, Nguyen TD. Scleral anisotropy and its effects on the mechanical response of the optic nerve head. *Biomechanics and Modeling in Mechanobiology*. 2013;12:941–963.
19. Sigal IA, Bilonick RA, Kagemann L, et al. The optic nerve head as a robust biomechanical system. *Invest Ophthalmol Vis Sci*. 2012;53:2658–2667.
20. Candiello J, Balasubramani M, Schreiber EM, et al. Biomechanical properties of native basement membranes. *FEBS J*. 2007;274:2897–2908.
21. Kaufmann C, Bachmann LM, Robert YC, Thiel MA. Ocular pulse amplitude in healthy subjects as measured by dynamic contour tonometry. *Arch Ophthalmol*. 2006;124:1104–1108.
22. Nelson ES, Mulugeta L, Myers JG. Microgravity-induced fluid shift and ophthalmic changes. *Life*. 2014;4:621–665.
23. Silver DM, Geyer O. Pressure-volume relation for the living human eye. *Curr Eye Res*. 2000;20:115–120.
24. Magnaes B. Body position and cerebrospinal fluid pressure. Part 2: clinical studies on orthostatic pressure and the hydrostatic indifferent point. *J Neurosurg*. 1976;44:698–705.
25. Magnaes B. Body position and cerebrospinal fluid pressure. Part 1: clinical studies on the effect of rapid postural changes. *J Neurosurg*. 1976;44:687–697.
26. Ren R, Jonas JB, Tian G, et al. Cerebrospinal fluid pressure in glaucoma: a prospective study. *Ophthalmology*. 2010;117:259–266.
27. Nikkhah H, Feizi M, Abedi N, Karimi S, Yaseri M, Esfandiari H. Choroidal Thickness in Acute Non-arteritic Anterior Ischemic Optic Neuropathy. *J Ophthalmic Vis Res*. 2020;15:59–68.
28. Morrison JC, Pollack IP. *Glaucoma Science and Practice*. New York, NY: Thieme Medical Publishers; 2003.
29. Mollan SP, Davies B, Silver NC, et al. Idiopathic intracranial hypertension: consensus guidelines on management. *J Neurol Neurosurg Psychiatry*. 2018;89:1088–1100.
30. Wall M, Corbett JJ. Revised diagnostic criteria for the pseudotumor cerebri syndrome in adults and children. *Neurology*. 2014;83:198–199.
31. Mader TH, Gibson CR, Pass AF, et al. Optic disc edema in an astronaut after repeat long-duration space flight. *J Neuroophthalmol*. 2013;33:249–255.
32. Khanna RK, Pham CJ, Malik GM, Spickler EM, Mehta B, Rosenblum ML. Bilateral superior ophthalmic vein enlargement associated with diffuse cerebral swelling. Report of 11 cases. *J Neurosurg*. 1997;86:893–897.
33. Liguori C, Romigi A, Albanese M, et al. Revised diagnostic criteria for the pseudotumor cerebri syndrome in adults and children. *Neurology*. 2014;82:1752–1753.
34. Mckay MD, Beckman RJ, Conover WJ. Comparison of 3 Methods for Selecting Values of Input Variables in the Analysis of Output from a Computer Code. *Technometrics*. 1979;21:239–245.
35. Schwaner SA, Feola AJ, Ethier CR. Factors affecting optic nerve head biomechanics in a rat model of glaucoma. *J R Soc Interface*. 2020;17:20190695.
36. Grytz R, Downs JC. A forward incremental prestressing method with application to inverse parameter estimations and eye-specific simulations of posterior scleral shells. *Comput Methods Biomech Biomed Engin*. 2013;16:768–780.
37. Jin Y, Wang X, Zhang L, et al. Modeling the Origin of the Ocular Pulse and Its Impact on the Optic Nerve Head. *Invest Ophthalmol Vis Sci*. 2018;59:3997–4010.
38. Wang X, Teoh CKG, Chan ASY, Thangarajoo S, Jonas JB, Girard MJA. Biomechanical Properties of Bruch's Membrane-Choroid Complex and Their Influence on Optic Nerve Head Biomechanics. *Invest Ophthalmol Vis Sci*. 2018;59:2808–2817.
39. Arnold AC. Pathogenesis of nonarteritic anterior ischemic optic neuropathy. *J Neuroophthalmol*. 2003;23:157–163.
40. Arnold AC, Hepler RS. Fluorescein angiography in acute nonarteritic anterior ischemic optic neuropathy. *Am J Ophthalmol*. 1994;117:222–230.
41. Tesser RA, Niendorf ER, Levin LA. The morphology of an infarct in nonarteritic anterior ischemic optic neuropathy. *Ophthalmology*. 2003;110:2031–2035.
42. Mansour AM, Shoch D, Logani S. Optic disk size in ischemic optic neuropathy. *Am J Ophthalmol*. 1988;106:587–589.
43. Chan CK, Cheng ACO, Leung CKS, et al. Quantitative assessment of optic nerve head morphology and retinal nerve fibre layer in non-arteritic anterior ischaemic optic neuropathy with optical coherence tomography and confocal scanning laser ophthalmoloscopy. *Br J Ophthalmol*. 2009;93:731–735.
44. Contreras I, Rebolleda G, Noval S, Munoz-Negrete FJ. Optic disc evaluation by optical coherence tomography in nonarteritic anterior ischemic optic neuropathy. *Invest Ophthalmol Vis Sci*. 2007;48:4087–4092.

Investigative Ophthalmology & Visual Science

45. Yang Y, Zhang H, Yan Y, Gui Y, Zhu T. Comparison of optic nerve morphology in eyes with glaucoma and eyes with non-arteritic anterior ischemic optic neuropathy by Fourier domain optical coherence tomography. *Expl Ther Med*. 2013;6:268–274.
46. Feola AJ, Coudrillier B, Mulvihill J, et al. Deformation of the Lamina Cribrosa and Optic Nerve Due to Changes in Cerebrospinal Fluid Pressure. *Invest Ophthalmol Vis Sci*. 2017;58:2070–2078.
47. Burgoyne CF. A biomechanical paradigm for axonal insult within the optic nerve head in aging and glaucoma. *Exp Eye Res*. 2011;93:120–132.
48. Campbell IC, Coudrillier B, Ethier CR. Biomechanics of the posterior eye: A critical role in health and disease. *J Biomech Eng*. 2013;136:021005.
49. Barnett M, Sinha MD, Morrison D, Lim M. Intracranial hypertension presenting with severe visual failure, without concurrent headache, in a child with nephrotic syndrome. *BMC Pediatrics*. 2013;13:167.
50. Downs JC. IOP telemetry in the nonhuman primate. *Exp Eye Res*. 2015;141:91–98.
51. Downs JC, Burgoyne CF, Seigfreid WP, Reynaud JF, Strouthidis NG, Sallee V. 24-hour IOP telemetry in the nonhuman primate: implant system performance and initial characterization of IOP at multiple timescales. *Invest Ophthalmol Vis Sci*. 2011;52:7365–7375.
52. Akbulut S, Pekel G, Pekel E, Cetin EN. Alterations in retinal and choroidal thickness following nonarteritic anterior ischemic optic neuropathy. *Intl Ophthalmol*. 2021;41:2723–2728.
53. Li H, Sun J, Wang H, Wang Y, Wang Z, Li J. Evaluation of hemodynamic changes in nonarteritic anterior ischemic optic neuropathy using multimodality imaging. *Quant Imaging Med Surg*. 2021;11:1932–1945.
54. Ling JW, Yin X, Lu QY, Chen YY, Lu PR. Optical coherence tomography angiography of optic disc perfusion in non-arteritic anterior ischemic optic neuropathy. *Int J Ophthalmol*. 2017;10:1402–1406.
55. Wang H, Meng ZY, Li SG, Wang JJ, Sun J, Li HY. Macular evaluation of the retinal and choroidal vasculature changes in anterior ischemic optic neuropathy-a case control study. *BMC Ophthalmol*. 2018;18:341.
56. Candiello J, Cole GJ, Halfter W. Age-dependent changes in the structure, composition and biophysical properties of a human basement membrane. *Matrix Biol*. 2010;29:402–410.